Large-Scale Nanophotonic Structures for Long-Term Monitoring of Cell Proliferation

doi: info:doi/10.1002/adbi.201700258

DOI: 10.1002/((please add manuscript number))
Article type: Communication

Title: Large-scale nanophotonic structures for long-term monitoring of cell proliferation

*Nikhil Bhalla, Shivani Sathish, Abhishek Sinha and Amy Q. Shen**

Dr. N. B. Author 1, S.S. Author 2, A.S. Author 3, Prof. A.Q.S. Author 4

Micro/Bio/Nanofluidics Unit, Okinawa Institute of Science and Technology Graduate University, 1919-1 Tancha, Onna, Kunigami District, Okinawa Prefecture 904-0495, Japan

*E-mail: amy.shen@oist.jp
Prof. A.Q.S. Author 4
Micro/Bio/Nanofluidics Unit, Okinawa Institute of Science and Technology Graduate University, 1919-1 Tancha, Onna, Kunigami District, Okinawa Prefecture 904-0495, Japan

Keywords: biosensors, cell proliferation, LSPR, nanoplasmons, nanomushrooms

Abstract

Innovative sensing materials have enabled the discovery of cell biology principals at nanoscale. In order to evaluate cell behavior and responses, it is necessary to accurately monitor cell proliferation. However, it remains challenging to develop nanomaterials possessing pertinent properties for sensing, while ensuring cell survival and unaltered cellular responses long term. This work develops highly sensitive, large-scale and bio-compatible nanoplasmonic biosensors for long term monitoring of cell proliferation, reported for the first time. The nanoplasmonic sensor consists of mushroom-like structures, with stems of silicon dioxide and caps of gold, ~ 20 nm in width and 45-60 nm in total height, and an average spacing of 10 nm, covering a total surface area of 18.75 cm^2. The localized surface plasmons on the nanomushroom caps are exploited to monitor proliferating fibroblast cells. Changes in nanoplasmonic resonances of the nanomushrooms are directly proportional to the number of cells that bound to them. Fibroblast proliferation was successfully monitored for 7 days, demonstrating remarkable bio-compatibility of the nanomushroom substrates. These nanomushroom substrates preserves cell viability and serves as a label-free platform for long-term monitoring of cell proliferation. Our results also open new opportunities in developing standard cell assays without chemical labels to detect cellular responses at nanoscale.

Main text

Cell proliferation is a fundamental process in living organisms, from the start of embryogenesis until death[1]. In medical research, monitoring cell division is essential to investigations of the health and functions of cells and tissues. This need has motivated the development of cell proliferation assays[2], commonly based on four methodologies: (1) measurement of total DNA[3]; (2) detection of cell proliferation markers[4]; (3) analysis of metabolic activities [5]; and (4) measurement of ATP content during cell growth [6]. All these assays are considered as "labeled" assays that rely on luminescence[7], fluorescence[8], colorimetry[9] (mostly dyes) or radioactive tags[10] to monitor cellular activities related to cell proliferation. Unfortunately, the choice and performance of labeled assays tend to be constrained by: (1) the cellular expression of a given cell type, and (2) the availability of tags for specific cell expression. In most of the labeled assays, "signal quenching" is often associated with false experimental positives[11], which decreases assay reliability. Furthermore, labeled assays are laborious, costly, unsuitable for real time cell analysis, and sometimes require the usage of toxic reagents, such as radioactive labels[12].

Label-free biosensors utilize biophysical properties of a given analyte, such as its mass (e.g., in quartz crystal microbalance), refractive index (e.g., in plasmonic nanobiosensors), or molecular charge (e.g., in potentiometric and amperometric sensors) to monitor the response of the analyte in real-time[13]. Recently, nanomaterial-based label-free photonic biosensors have revealed unprecedented information on DNA and protein molecular interactions[14]. However, few attempts have been made to apply label-free photonic biosensors to cellular assays, as it is challenging to develop nanostructured substrates with large surface areas that promote both sensing and long term cell survival. In addition, photonic techniques have been coupled with microscopy tools to enhance live cell imaging and distinguish different types of cell behavior such as cell activation, adhesion, proliferation, migration and apoptosis[15]. In contrast to these 'imaging' based techniques, 'sensor' based techniques generate average

responses proportional to concentrations of a given analyte. Such an average response captures real time kinetics of cell behavior. In this work, we develop novel nanoplasmonic mushroom-like structures (NM based sensors) for label free, long-term cell proliferation detection with high sensitivity, on a large interrogation area, specifically suitable for clinically relevant cell experiments (e.g., drug testing) that require large interrogation areas involving standard 96 well assay plates. Thus the unique features of our NM based sensors can be complementary to imaging based tools to probe cells behavior.

The developed nanomushroom (NM) structures are 45-60 nm in height and ~20 nm in width, evenly distributed with ~10 nm spacing on a standard glass slide (25 mm × 75 mm). Each NM consists of a silicon dioixde (SiO_2) stem of 30-40 nm in height, and a gold (Au) cap of 15-20 nm in thickness (Figure 1a). These structures were fabricated by a simple, high-throughput, 3-step process. A thin Au film (4 nm) was first deposited on a SiO_2 substrate (Figure 1a. (i,ii)), followed by thermal dewetting of the Au film at 560^oC for 3 hr (Figure 1a. iii). Upon thermal dewetting, the gold film breaks into nanoisland-like structures (Figure 1a. iii). Finally, Au nanoislands were exposed to reactive SF_6 ion plasma, which selectively etches away SiO_2 to create nanomushroom pillar-like structures (see more details in SI-Section 1).

Upon exposure to white light (350-800 nm), collective oscillations of free electrons were observed on the gold caps of the NM structures. These oscillations are known as localized surface plasmon resonances (LSPR). Here, LSPR is enhanced by lifting metal Au nanostructures above substrates with dielectric pillars (present in our NM structures), elevating local electromagnetic (EM) fields around the nanostructures. This is primarily due to an increase in the refractive index sensitivity of the resultant LSPR sensors, as a large fraction of the spatial region with enhanced electric fields is easily accessible by molecular species that bind on the substatres[16]. Furthermore, the transparent SiO_2 substrate on which NMs are fabricated, allows LSPR resonances to be measured in transmission (T) mode (T-LSPR) (Figure 1b). T-LSPR sensing mode offers the potential to develop high-performance

integrated devices at low cost and with a user-friendly optical setup for direct imaging[17]. LSPR instrumentation details are provided in SI-Section 2. Figure 1c shows typical LSPR characterstics of our NM substrate, resonating at ~532.5 nm. Due to the high-order symmetry of spherical gold caps of the NM structures (size distribution shown in figure 1a, iv) and the use of a 'single' angle of incidence, these NM structures exhibit an optical response of a 'single' plasmonic mode (transverse mode at ~532.5 nm, as shown in figure 1c). While the absorption spectrum, characterized by a peak at ~532.5 nm, is based on the transverse mode of the NM (electron oscillation along the short axis, 500–700 nm), extinction tail extending to the infrared region based on the longitudinal mode (electron oscillation along the long axis, ≥~700 nm) may be observed at different angles of incidence. However, for long term (e.g., 7 days) cell experiments, excitation in the visible in comparison to near infrared (NIR) regimes induces less stress on cells. Therefore transverse mode characterized by a peak at ~532.5 nm is used for LSPR based detection of cell proliferation events. This transverse mode of LSPR is highly sensitive to the refractive index (RI) of the surrounding medium (e.g., solvent /analyte/cells), enabling detection of binding events on the nanostructures. Our NM LSPR sensor was characterized for RI sensitivity by using 4 solutions with known RI: water (RI=1.330), acetone (RI=1.3590), ethanol (RI=1.361), and isopropanol (RI=1.3776) (Figure 1d). NM sensor exhibits a sensitivity of 83.15 nm/RIU, deduced from the slope of the wavelength versus the refractive index plot (Figure 1d). This sensitivity is reasonably good for a large sensor substrate containing spherical gold nanostructures for LSPR applications, with reported range of 20-96 nm/RIU[18]. It is possible to improve the sensitivity of the NM sensor by modifying fabrication parameters (such as initial thickness of gold film and time of exposure to plasma) to optimize the NM size and spacing. Changes in NM geometry will lead to a change in LSPR response. The condition $R/\lambda < 0.1$, where R is the radius of the nanostructure and λ is the wavelength of the incident light, should be satisfied for LSPR[19]. The LSPR sensitivity can be enhanced by reducing the ratio of R/λ, i.e., decreasing the size of the nanostructure with fixed

wavelength[19]. The second parameter to consider in our NM geometry is the periodicity of the nanostructures where decreasing the gap of the nanostructures leads to enhanced sensitivity of the LSPR[20]. More systematic studies are required in the future to optimize the size and distribution of NM structures for enhanced sensitivty of the NM based biosensor.

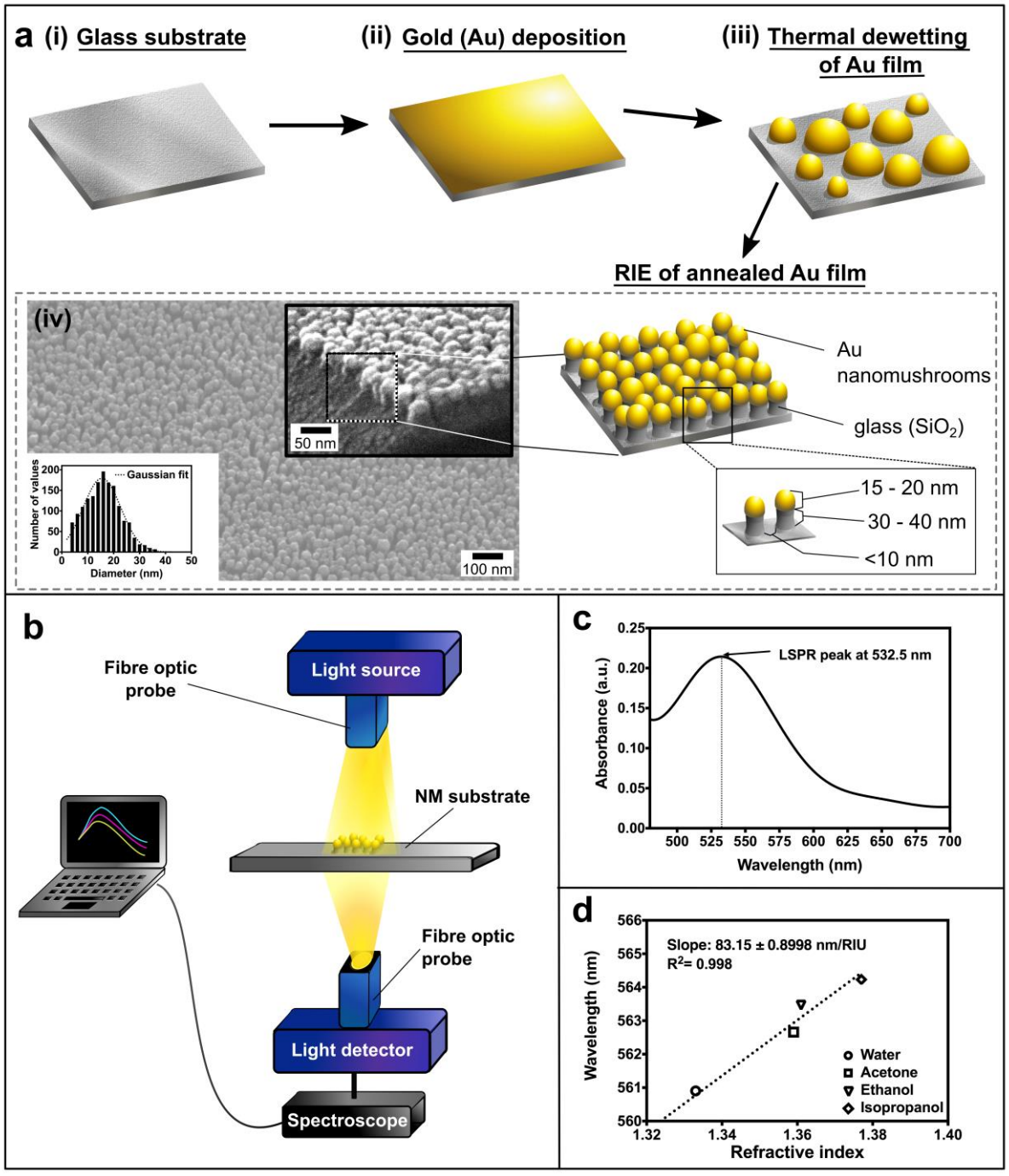

Figure 1. *Characterization of nanomushroom (NM): a) The nanomushroom fabrication process includs: i) glass substrate; ii) depositing gold (Au) on a glass substrate; iii) Au*

nanoislands formed by thermal dewetting of Au film annealed at 560^{o}C for 3 hr; iv) Exposing Au nanoislands under reactive ion etching plasma of SF_6 ions to produce Au NM. Left: The SEM image (FEI Quanta 250 FEG) of a NM substrate acquired at 30 kV and 70.5kX. The inset shows the cross-section image of the NM substrate, captured at 30 kV and 250kX and the size distribution of NM. Right: The schematic shows the size and spacing of NMs. b) Transmission-Localized Surface Plasmon Resonance (T-LSPR) mode to acquire LSPR signals from a NM substrate. c) Wavelength versus absorbance curve showing the characteristic LSPR peak of a NM substrate. d) Optical characteristics of NM substrates when exposed to solutions with different refractive indices (RI): DI-water (RI=1.3330), Acetone (RI=1.3590), Ethanol (RI=1.361) and IPA (RI=1.3776).

To demonstrate the utility of the NM substrate in cellular response detection, proliferation of fibroblasts (NIH 3T3) was monitored and quantified for 7 days. NIH 3T3 cells were choosen since this cell line is commonly used to validate cell fuctionality *in-vitro*[21]. The suitability of our NM substrate for cell adhesion[22] was first validated by examining microscale cellular morphology using scanning electron microscopy (SEM). Cells were fixed with paraformaldehyde to preserve their structures after 48 hr of incubation on a NM substrate, and then sputtered with a thin layer of a palladium-platinum mixture for easy visualization under SEM (Figure 2a (i,ii)). Fibroblasts adhered well to the NM substrate (see Figure 2(b,c)). Filopodia (finger-like structures) are also observed on adherent cells (Figure 2d), indicating that fibroblasts maintained active cellular processes after adhering to the NM substrate. Filopodia function as antennae, enabling the cells to probe their local envionments, migrate, and communicate with neighboring cells during cell growth. Figure 3 shows the response of the NM substrate to the proliferation of fibroblast cells. Figure 3(a-d) are phase-contrast microscopy images of fibroblast cells during proliferation on a NM substrate at different time intervals, depicting cell morphologies characteristic of migrating cells[23]. This visual

evidence validated the biocompatibility of the NM substrate for fibroblast survival for 168 hrs (7 days), demonstrating the potential of NM substrates for long-term cell assay experiments.

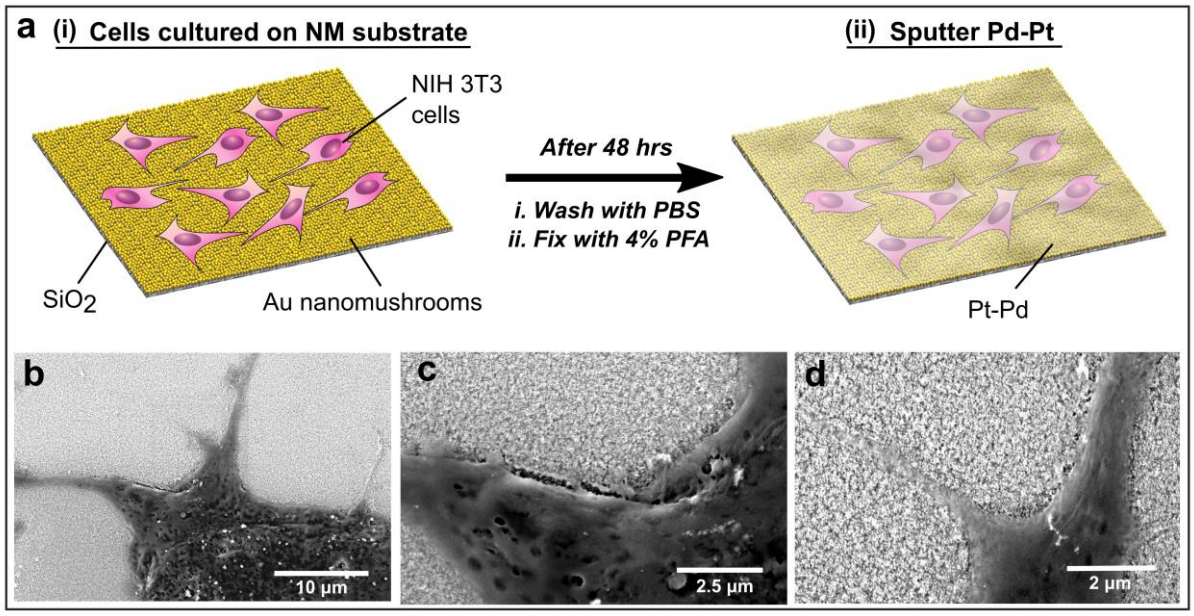

Figure 2. *Cell growth and imaging on a NM substrate: a) Schematic illustration of fibroblast adhesion and SEM imaging techniques on a NM substrate. b & c) SEM images of fibroblasts adhere and d) form filopodia on the NM substrate (Zeiss SEM, 5 kV, with 17kX to 25kX magnifications).*

The proliferation of fibroblast cells was detected and characterized by LSPR signals on NM sensors. The LSPR detection is determined by the decay length of the electro-magnetic field of localized plasmons which is around ~ 10 nm. Henceforth, the NM sensor can only measure changes in the refractive index within 10 nm from its surface. In parallel, new cells formed during cell proliferation adhere on the NM sensor substrates via membrane proteins (e.g. focal adhesion proteins) that aid in cell adhesion[23]. This implies that regions within distances of 10 nm above the NM sensor surface are dominated by membrane proteins that aid in adhesion. Therefore, the NM sensor essentially detects the proliferation of cells with high specificity by measuring the new cells adhering to the substrate via the membrane proteins, as validated in the sensor response plots on figure 3e-l. For each given time, 3 different sensor chips were used to collect the LSPR signals (wavelength shifts $\Delta\lambda$ and absorbance) while the area in a

given sample was kept fixed for the whole duration of the experiment, representing the mean and standard error values, see figure 3 e-h, j. During the initial phase of the experiment, the surface coverage of cells on NM substrates increases over time due to cell spreading (SI-Section 3), which changes the local refractive index of the NMs, causing wavelength shifts in the LSPR response. Figure 3e displays changes in the wavelength and mRIU (milli refractive index unit) of LSPR in a NM substrate for a control sample with pure culture media (red symbols) and NIH 3T3 cells in the culture media (blue symbols) during the entire course of the 7 day experiment. These wavelength changes ($\Delta\lambda$) are extracted from normalized absorbance *versus* wavelength plots of the NM LSPR signal (more details in SI-Section 4). The distinct difference in the LSPR wavelength shift between the blue and red symbols suggests that proliferation events (adhesion, spreading and then cell division) induced changes in the resonance properties of LSPR signal. In addition, the peak wavelength of LSPR shifts toward the right side of the UV-VIS spectrum (redshift) after 1 day, showing a decreased LSPR response. Figure 3f demonstrates the absorption intensity changes of LSPR for both pure culture media and cell suspensions for 7 days. While $\Delta\lambda$ response difference between the cell suspension and the control samples is significant, there is less than 0.2 unit change in the LSPR absorption intensity, see red and blue symbols in Figure 3f. This small variation in the absorbance comes from small changes in the content of culture media (due to the consumption of proteins by cells during the proliferation) during the 7-day period.

We then replotted the 7-day data from Figure 3 e&f in two separate figures to highlight the cell proliferation behavior within and after the first 24 hrs. Since the frequency is inversely proportional to the wavelength, changes in LSPR peak shifts can be described in terms of LSPR frequency change. During the initial stages of the cell proliferation (< 15 hr), as shown in figure 3g, the charge localization effects[13d],[24] (accumulation of surface charges on NMs due to cell spreading/adhesion) increase the frequency of the LSPR (or decrease the wavelength). However, when the cell number starts to increase over a period of 7 days, the

proliferated cells on the NM substrate elevate the optical extinction coefficient of NMs at the resonant frequency. This leads to confinement and concentration of electromagnetic energy in the form of dielectric fields on the surface of the NM structures[25]. Thereafter, a decrease in the frequency of the LSPR, i.e., an increase in the wavelength (redshift), is observed in the LSPR peak, as seen from figure 3h.

We also measured the sensor response to cells during the first 1.5 hr (90 minutes) of the experiment, investigating the effect of protein/ growth factors on the LSPR signal changes. An insignificant change in the wavelength shift (< 0.3 nm) was observed during the first hour of incubation (Figure 3i), confirming that adhesion or cell secretions events did not drive the RI changes of the NM sensor observed in Figure 3e, verifying that NM wavelength changes mainly correspond to the increasing surface coverage of divided cells on the NM substrate. The wavelength response of LSPR was also quantified and correlated with both cell number changes and normalized cell numbers observed on the NM surface (Figure 3j-l). The Au NM substrates were washed twice with 1x PBS after an LSPR measurement was taken. Next, 1 mL of 0.5% trypsin was added to strip cells. The number of cells was then counted using a hemocytometer (Bright-Line, USA).

Figure 3j shows that LSPR signal changes proportionally as the cell number increases during the 7-day measurement period. By extracting the wavelength change $\Delta\lambda$ and the cell number from figure 3j, we demonstrate that our NM sensors can also be used for counting cells during the course of the cell proliferation experiment (figure 3k-l). Figure 3k shows the direct change in the cell number ($N^* = nf - ni$) versus the wavelength change $\Delta\lambda$. Here n_f is the measured cell number at a given time interval, and n_i is the initial seeded number. Figure 3l plots the normalized cell number ($N=n_f/n_i$) that is defined as the ratio of n_f over n_i. The limit of detection (LOD)[33] of the NM sensor was estimated to be ~ 0.16 nm (see details in SI-Section 5), implying that our sensor can reliably detect a change of 160 cells upon

proliferation for an intial seeded 10,000 cells, or more generally, 1.6% of cells in a given cell population.

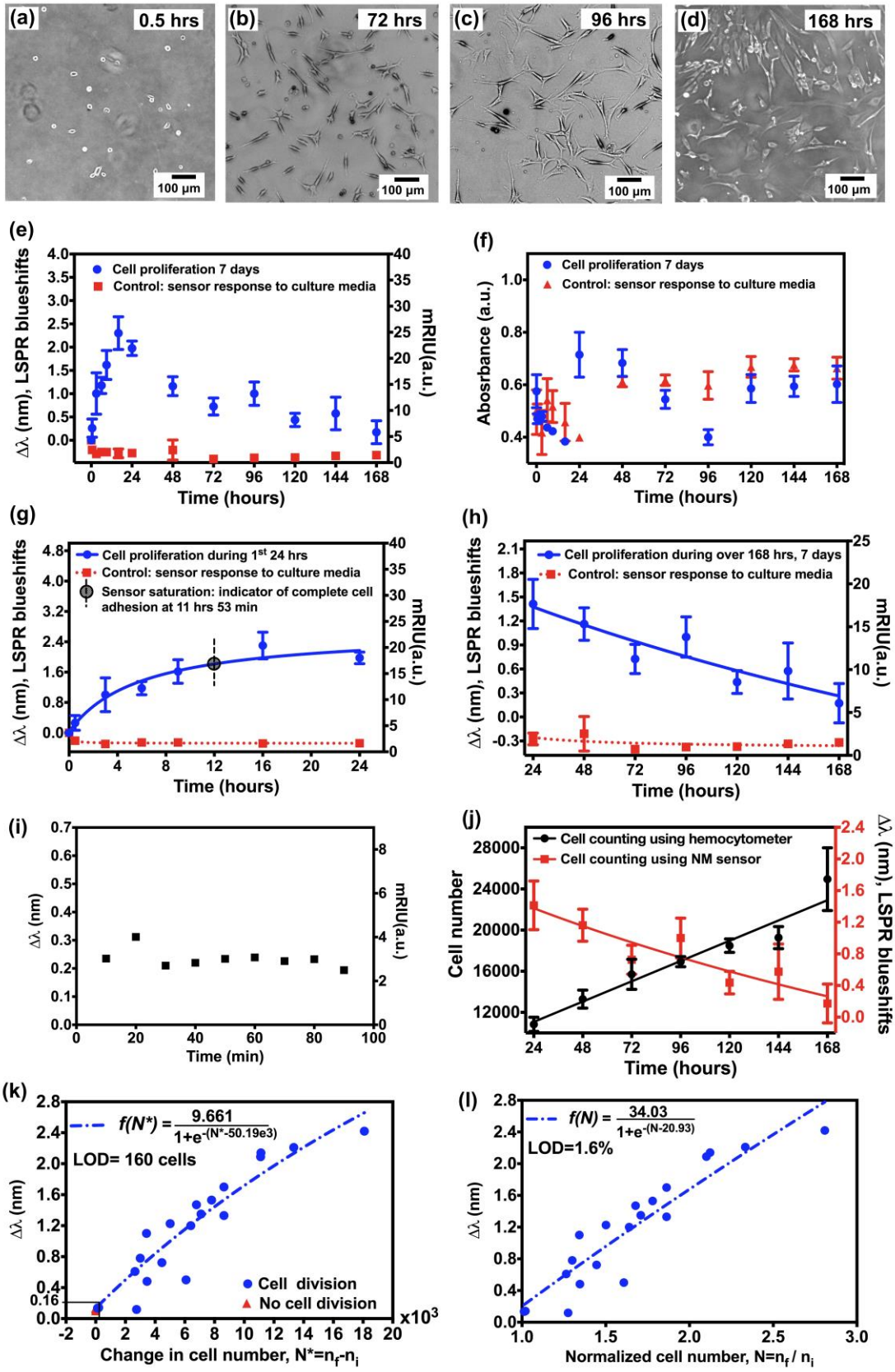

Figure 3. *LSPR response of NM sensors during the cell proliferation process. a-d) Phase-contrast images (Olympus CKX41) of NIH 3T3 cells on NM substrates at different time intervals. e) Wavelength changes* $\Delta\lambda$ *(blueshift) and f) absorbance response during the entire 7 day experiment. g) Wavelength (blueshift) and refractive index response for the intial 24 hours, h) for 24 hr-- 7 days, and i) the intial 1.5 hr of cell incubation. j) Correlation between the cell number and LSPR wavelength shifts* $\Delta\lambda$ *during the 7 day experiment. For a fixed time, 3 data points are recorded from 3 different sensors. k) Changes in the cell number* $N^* = n_f - n_i$, *versus* $\Delta\lambda$ *(redshifts) during the period of 24-168 hrs.* n_f *is the measured cell number at a given time, while* n_i *is the intital seeding number. Note that in e-h,j, recorded data represent the mean and standard error values obtained from at least 3 sensors. l) Normalized cell number N (*$N=n_f/n_i$*) versus* $\Delta\lambda$ *(redshifts) of the NM substrate over a period of 24-168 hrs.*

The dotted logistic fit of the experimental data (Figure 3l) serves as a proof of concept for quantifying cell numbers during the NIH/3T3 cell proliferation experiment using our NM sensor. On a relevant application for general label free cell counting, a calibration curve of NM LSPR response versus known cell numbers can be constructed. However, every cell type will exhibit a different LSPR response, depending on the size and overall charge of the cells, thus such calibration curve is specific to cell types. The developed NM sensor has a unique advantage of obtaining real time information on cell numbers for long term cell proliferation studies, by avoiding striping of cells from a substrate when compared to hemocytometers (conventional cell counters), after initial calibration curve is constructed (e.g. fig 3l) for a given cell type. In addition, our NM sensors offer portability at comparable cost in comparison to the existing cell counting techniques.

In summary, using gold and glass we engineered nanophotonic structures bearing sub-20-nm mushroom-like pillar arrays with properties desirable for both LSPR sensing and living cell assays. The developed NM sensor detects changes in the RI caused by cell division, enabling analysis of molecular and other cell functions measurable in real time. In addition,

our NM substrates are ‘scalable‘ owing to the ease of integration with emerging technologies such as CMOS[26], microfluidics[27], wireless systems, and nanosystem packaging[28]. For example, if an LSPR biosensor is integrated with a wireless readout on a mobile phone[29], it will allow users to readily quantify cell numbers remotely without physical intervention, minimizing unwanted contamination. Compared with electrical sensors, our optical method exposes cells with light in the visible regime of the spectrum, which minimizes alteration in cell response as it avoids exposure to unwanted energies (such as electric fields or high energy light) during the long term (e.g. 7 days) measurement. With these advantages, our NM sensor possesses promising potentials to develop new design strategies for next-generation cell assay tools.

Experimental Section

SEM and regular cell imaging: Scanning electron microscopy (Scanning Electron Microscope FEI Quanta 250 FEG) was used to image the cell on nanomushroom (NM) structures at 30kV with a magnification of 253.5kX. Prior to imaging, nanostructures were coated with palladium-platinum (Pd-Pt) using ion sputtering (Ion Sputter MC1000) to avoid sample charging. To verify the adhesion and biocompatibility between cells and the NM substrate, after the cultured cells had adhered to the NM substrate for 48 hr, they were fixed by incubating with boiling (90°C) 4% paraformaldehyde (PFA) for 1 minute, followed by washing with phosphate-buffered saline (PBS). Cells on the NM substrate were then coated with a thin layer of Pd-Pt and imaged using a low-voltage SEM (Zeiss SEM) at 5 kV at various magnifications from 17kX to 25kX. Images of cells were also recorded during the cell proliferation experiments, using an Olympus CKX41 phase-contrast inverted microscope with a DP27-A camera system.

Cell assays: Nanomushroom substrates were placed into 35 mm (9 cm^2) Corning cell culture dishes. NM substrates were sterilized with isoproponal and 70% ethanol, and allowed to dry in the cell-culture biosafety cabinet under UV light. NM substrates were coated with Poly D

Lysine (PDL) solution (0.003% in PBS, 500 μL / substrate) and placed in a cell culture incubator, with humidified environment at 37ºC and 5% CO_2, for 30 minutes. Dishes were then pre-filled with 1 mL of Dulbecco's Modified Eagle Medium (DMEM) high glucose supplemented with 10% calf serum. NIH/3T3 fibroblasts were next seeded in the dish at low densities (~ 10,000 cells per NM substrate). Cell culture media was then added to wells at a final volume of 2 mL. An LSPR reading was immediately taken. Cells were allowed to grow in the cell culture incubator for a given period of time. No new cell-culture medium was added to or removed from the dish during the 7-day duration of the experiment.

Acknowledgements

Authors would like to thank Dr. Steve Aird at OIST for careful proof reading, for Dr. Guillaume Vares and Mr. Hsieh-Fu Tsai at OIST for fruitful discussions. The authors also acknowledge financial support from the OIST Graduate University with subsidy funding from the Cabinet Office, Government of Japan.

Received: ((will be filled in by the editorial staff))
Revised: ((will be filled in by the editorial staff))
Published online: ((will be filled in by the editorial staff))

References

[1] aJ. J. Heit, S. K. Karnik, S. K. Kim, *Annu. Rev. Cell Dev. Biol.* **2006**, *22*, 311-338; bS. Y. Lunt, M. G. Vander Heiden, *Annual review of cell and developmental biology* **2011**, *27*, 441-464.
[2] D. S. Chen, I. Mellman, *Nature* **2017**, *541*, 321-330.
[3] A. Salic, T. J. Mitchison, *Proceedings of the National Academy of Sciences* **2008**, *105*, 2415-2420.
[4] N. Raab-Traub, K. Flynn, *Cell* **1986**, *47*, 883-889.
[5] C. F. Labuschagne, N. J. Van Den Broek, G. M. Mackay, K. H. Vousden, O. D. Maddocks, *Cell reports* **2014**, *7*, 1248-1258.
[6] T. L. Riss, R. A. Moravec, A. L. Niles, S. Duellman, H. A. Benink, T. J. Worzella, L. Minor, *Cell Viability Assays***, 2016**.
[7] P. E. Andreotti, I. A. Cree, C. M. Kurbacher, D. M. Hartmann, D. Linder, G. Harel, I. Gleiberman, P. A. Caruso, S. H. Ricks, M. Untch, *Cancer research* **1995**, *55*, 5276-5282.

[8] M. H. Wade, J. E. Trosko, M. Schindler, *Science* **1986**, *232*, 525-529.
[9] F. Denizot, R. Lang, *Journal of immunological methods* **1986**, *89*, 271-277.
[10] R. Liu, S. Zhang, C. Wei, Z. Xing, S. Zhang, X. Zhang, *Accounts of chemical research* **2016**, *49*, 775-783.
[11] J. R. Huth, R. Mendoza, E. T. Olejniczak, R. W. Johnson, D. A. Cothron, Y. Liu, C. G. Lerner, J. Chen, P. J. Hajduk, *Journal of the American Chemical Society* **2005**, *127*, 217-224.
[12] A. M. Cohen, J. F. Burdick, A. S. Ketcham, *The Journal of Immunology* **1971**, *107*, 895-898.
[13] aX. Yu, L. Shi, D. Han, J. Zi, P. V. Braun, *Advanced Functional Materials* **2010**, *20*, 1910-1916; bS. A. Maier, M. L. Brongersma, P. G. Kik, S. Meltzer, A. A. Requicha, H. A. Atwater, *Adv Mater* **2001**, *13*, 1501-1505; cS. Myung, A. Solanki, C. Kim, J. Park, K. S. Kim, K. B. Lee, *Adv Mater* **2011**, *23*, 2221-+; dJ. N. Anker, W. P. Hall, O. Lyandres, N. C. Shah, J. Zhao, R. P. Van Duyne, *Nature Materials* **2008**, *7*, 442-453; eK. V. Sreekanth, Y. Alapan, M. ElKabbash, E. Ilker, M. Hinczewski, U. A. Gurkan, A. De Luca, G. Strangi, *Nature Materials* **2016**, *15*, 621-+.
[14] L. Mou, X. Jiang, *Advanced Healthcare Materials* **2017**.
[15] aW. L. Chen, K. D. Long, J. Kurniawan, M. Hung, H. J. Yu, B. A. Harley, B. T. Cunningham, *Adv Opt Mater* **2015**, *3*, 1623-1632; bW. L. Chen, K. D. Long, M. Lu, V. Chaudhery, H. Yu, J. S. Choi, J. Polans, Y. Zhuo, B. A. C. Harley, B. T. Cunningham, *Analyst* **2013**, *138*, 5886-5894.
[16] Y. Shen, J. H. Zhou, T. R. Liu, Y. T. Tao, R. B. Jiang, M. X. Liu, G. H. Xiao, J. H. Zhu, Z. K. Zhou, X. H. Wang, C. J. Jin, J. F. Wang, *Nat Commun* **2013**, *4*. *2381*.
[17] W. Li, J. Xue, X. Jiang, Z. Zhou, K. Ren, J. Zhou, *RSC Advances* **2015**, *5*, 61270-61276.
[18] H. Chen, X. Kou, Z. Yang, W. Ni, J. Wang, *Langmuir* **2008**, *24*, 5233-5237.
[19] E. Petryayeva, U. J. Krull, *Anal Chim Acta* **2011**, *706*, 8-24.
[20] G. Y. Si, Y. H. Zhao, J. T. Lv, M. Q. Lu, F. W. Wang, H. L. Liu, N. Xiang, T. J. Huang, A. J. Danner, J. H. Teng, Y. J. Liu, *Nanoscale* **2013**, *5*, 6243-6248.
[21] A. Tang, J. Li, S. Zhao, T. Liu, Q. Wang, J. Wang, *Journal of Nanoscience and Nanotechnology* **2017**, *17*, 3888-3895.
[22] B. M. Gumbiner, *Cell* **1996**, *84*, 345-357.
[23] K. M. Yamada, S. S. Yamada, I. Pastan, *Proceedings of the National Academy of Sciences* **1976**, *73*, 1217-1221.
[24] N. Bhalla, N. Formisano, A. Miodek, A. Jain, M. Di Lorenzo, G. Pula, P. Estrela, *Biosensors and Bioelectronics* **2015**, *71*, 121-128.
[25] J. L. Hammond, N. Bhalla, S. D. Rafiee, P. Estrela, *Biosensors* **2014**, *4*, 172-188.
[26] aA. M. Hussain, M. M. Hussain, *Adv Mater* **2016**, *28*, 4219-4249; bB. Y. Zheng, Y. M. Wang, P. Nordlander, N. J. Halas, *Adv Mater* **2014**, *26*, 6318-6323.
[27] B. Xiong, K. M. Ren, Y. W. Shu, Y. Chen, B. Shen, H. K. Wu, *Adv Mater* **2014**, *26*, 5525-5532.
[28] M. Ganzhorn, A. Vijayaraghavan, A. A. Green, S. Dehm, A. Voigt, M. Rapp, M. C. Hersam, R. Krupke, *Adv Mater* **2011**, *23*, 1734-+.
[29] S. Dutta, K. Saikia, P. Nath, *Rsc Advances* **2016**, *6*, 21871-21880.
[30] N. Bhalla, D. Lee, S. Sathish, A. Q. Shen, *Nanoscale* **2017**, *9*, 547-554.